Published in final edited form as:
Cancer Discov. 2013 December ; 3(12): . doi:10.1158/2159-8290.CD-13-0310.

Activation of the PD-1 pathway contributes to immune escape in EGFR-driven lung tumors

Esra A Akbay[1,2,3,*], **Shohei Koyama**[2,4,*], **Julian Carretero**[5], **Abigail Altabef**[1,3], **Jeremy H Tchaicha**[1,2,3], **Camilla L Christensen**[1,2,3], **Oliver R Mikse**[1,2,3], **Andrew D Cherniack**[6], **Ellen M Beauchamp**[1,2], **Trevor J Pugh**[6], **Matthew D Wilkerson**[7], **Peter E Fecci**[8], **Mohit Butaney**[1], **Jacob B Reibel**[1,3], **Margaret Soucheray**[9], **Travis J Cohoon**[1,3], **Pasi A Janne**[1,2,10], **Matthew Meyerson**[1,2,6], **D. Neil Hayes**[7], **Geoffrey I Shapiro**[1,2], **Takeshi Shimamura**[9], **Lynette M Sholl**[11], **Scott J Rodig**[11], **Gordon J Freeman**[2,4], **Peter S Hammerman**[1,2,**], **Glenn Dranoff**[2,4,**], and **Kwok-Kin Wong**[1,2,3,10,**]

[1]Department of Medicine, Dana Farber Cancer Institute, Boston MA

[2]Harvard Medical School, Boston MA

[3]Ludwig Institute for Cancer Research, Boston, MA

[4]Department of Medical Oncology and Cancer Vaccine Center, Dana Farber Cancer Institute, Boston, MA

[5]Department of Physiology, University of Valencia, Valencia Spain

[6]Broad Institute, Cambridge MA

[7]UNC Lineberger Comprehensive Cancer Center, University of North Carolina at Chapel Hill, Chapel Hill, NC

[8]Department of Neurosurgery, Massachusetts General Hospital, Boston MA

[9]Oncology Institute, Department of Molecular Pharmacology and Therapeutics, Loyola University, Chicago IL

[10]Belfer Institute for Applied Cancer Science, Boston MA

[11]Department of Pathology, Brigham and Women's Hospital, Boston MA

Abstract

The success in lung cancer therapy with Programmed Death (PD)-1 blockade suggests that immune escape mechanisms contribute to lung tumor pathogenesis. We identified a correlation between Epidermal Growth Factor Receptor (EGFR) pathway activation and a signature of immunosuppression manifested by upregulation of PD-1, PD-L1, cytotoxic T lymphocyte antigen-4 (CTLA-4), and multiple tumor-promoting inflammatory cytokines. We observed decreased cytotoxic T cells and increased markers of T cell exhaustion in mouse models of EGFR-

[**]**Address correspondence to**: Kwok-Kin Wong, kwong1@partners.org, phone: 617-5827683, and fax: 617-5827839 Glenn Dranoff glenn_dranoff@dfci.harvard.edu, phone: 617-6325051, and fax: 617-6325167, or Peter Hammerman, peter_hammerman@dfci.harvard.edu, phone: 617-6325786, and fax: 617-6325167.
[*]These authors equally contributed to this work

COFLICT OF INTEREST DISCLOSURES

Gordon J. Freeman has patents and receives patent royalties on therapies involving PD-1.

Glenn Dranoff receives compensation as a consultant from Novartis, Merck, and Genentech, received research grants from Bristol-Myers Squibb and Novartis.

Pasi A. Janne receives compensation as a consultant from Boehringer Ingelheim, Roche, Genentech, Abbott, Astra-Zeneca, Pfizer, Sanofi, Chugai, and Clovis, and receives royalties from LabCorp.

driven lung cancer. PD-1 antibody blockade improved the survival of mice with EGFR-driven adenocarcinomas by enhancing effector T cell function and lowering the levels of tumor-promoting cytokines. Expression of mutant EGFR in bronchial epithelial cells induced PD-L1, and PD-L1 expression was reduced by EGFR inhibitors in non-small cell lung cancer cell lines with activated EGFR. These data suggest that oncogenic EGFR signaling remodels the tumor microenvironment to trigger immune escape, and mechanistically link treatment response to PD-1 inhibition.

INTRODUCTION

While genomic alterations that provide growth advantages to cancer cells are widely recognized to be essential for malignant transformation, discoveries made over the past decade suggest that evading immune destruction may also be critical for tumorigenesis (1). Mice lacking particular components of innate or adaptive immunity are more susceptible to spontaneous and carcinogen-induced tumors compared to wild type mice. Similarly, immunosuppressed patients develop both virus-induced and non-pathogen associated tumors more frequently than immunocompetent individuals (2). While these observations support the idea that immune mechanisms may suppress tumor development, tumor formation implies successful escape from immune control.

In order to generate efficient anti-tumor immune responses while maintaining self-tolerance, host reactions are tightly regulated through a combination of stimulatory and inhibitory signals. As T lymphocytes can recognize antigens derived from all cellular compartments presented in the context of surface major histocompatibility complex molecules, these anti-tumor effector cells have been the principal focus of cancer immunotherapy (3). Cytotoxic T lymphocyte associated antigen-4 (CTLA-4) is a critical negative immune checkpoint that limits the induction of potent cytotoxic T cell responses. Extensive clinical testing of human blocking anti-CTLA-4 monoclonal antibodies demonstrated an increase in anti-tumor immunity, with approximately 20% of metastatic melanoma patients achieving long-term survival; these substantive clinical benefits resulted in the FDA approval of ipilimumab as first or second line therapy for advanced melanoma (4). Based on these important results, a second negative immune checkpoint mediated through interactions of PD-1 with its ligands PD-L1 and PD-L2 has been investigated as a target for cancer immunotherapy. (5) Blocking antibodies against PD-1 or PD-L1 have demonstrated substantial clinical activity in patients with metastatic melanoma, renal cell carcinoma, non-small cell lung cancer, and other tumors (6, 7). Preliminary findings raise the possibility that PD-1 blockade might be less toxic than ipilimumab, although more detailed testing is required.

In the NSCLC clinical trials, only a subset of patients responded to PD-1 blockade, and early studies suggested that PD-L1 (*CD274*) expression may be a biomarker for therapeutic response to anti-PD-1 antibodies. While *PTEN* loss has been associated with increased *PD-L1* expression in gliomas (8), it is unknown whether specific genomic subsets of lung tumors utilize the PD-1 pathway as a mechanism of immune escape. One of the most commonly mutated oncogenes in NSCLC patients is *EGFR*. Previous studies have shown that activation of the EGFR pathway may be involved in suppressing the immune response in murine melanoma models either through activating regulatory T cells (Tregs) (9) or reducing the levels of the T cell chemo-attractant CCL27 (10).

Mutations in *EGFR* frequently arise in the kinase domain, rendering tumor cells sensitive to EGFR tyrosine kinase inhibitors (TKIs). However, despite the initial response, tumors invariably become resistant by either acquiring a secondary point mutation in EGFR (T790M) or additional alterations in other genes which bypass the need for ongoing

signaling from the mutated EGFR (11). A major focus in the therapy of EGFR-driven lung cancers is the development of therapeutic strategies that either delay acquired resistance or are effective in the setting of acquired resistance, though success in these areas has been limited to date. Based on the findings in the melanoma models and given that *EGFR* is one of the most commonly mutated oncogenes in NSCLC (12), we analyzed the immune microenvironment and a set of immunosuppressive pathways in *EGFR*-driven mouse lung tumors.

RESULTS

Activation of the EGFR pathway in murine bronchial epithelial cells leads to an immunosuppressive lung microenvironment

The two most frequently detected EGFR mutations in NSCLC patients are in the kinase domain: L858R substitution in exon 21 and deletions in a specific amino acid motif in exon 19 (Del19) (11). Similar to the patients carrying these mutations, mouse lung tumors carrying EGFR L858R or Del19 mutations initially respond to treatment with erlotinib (EGFR TKI) (13), followed by the development of resistance through acquired second site mutations (T790M). Separate mouse models carrying both the T790M and L858R or Del19 have been characterized (14, 15); while these do not respond to erlotinib therapy, they do respond to the mutant specific irreversible EGFR inhibitor WZ4002 for several weeks before they acquire resistance through other mechanisms (16). Microarray expression profiling of the mouse T790M/L858R (TL) tumors as compared to controls revealed increased levels of *Pd-1*, *Pd-l1* (*Cd274*), *Ctla-4*, *Il-6*, *Tgf-ß1*, and granulin (*Grn*) along with ligands for the EGFR (EGFR mutant vs WT for the gene set shown $p=3\times10^{-20}$) (Fig 1a). Analysis of microarray data from previously reported datasets showed no significant differences in *Pd-l1* and *Pd-l2* expression among tumors derived from multiple models of EGFR-driven lung adenocarcinoma (L858R, L858R/T790M (TL) and Exon 19 deletion/T790M (TD)) (17, 18), indicating that EGFR-driven tumors of a variety of *EGFR* mutations display elevated *Pd-l1* and *Pd-l2* expression as compared to normal lung (data not shown). We next confirmed the expression of PD-L1 on tumor ($CD45^{-}humanEGFR^{+}$) and associated hematopoietic cells by flow cytometry and immunohistochemistry in EGFR-driven mouse lung adenocarcinomas (IHC) (Fig 1b, Supplementary Fig 1).

As an initial step to understand the basis for compromised anti-tumor immunity in mice carrying EGFR-driven tumors, we analyzed the tumor microenvironment in comparison to the lungs from littermate controls to characterize the alterations associated with oncogene expression. Tumor infiltrating T cells displayed a significantly lower $CD8^{+}/CD4^{+}$ and $CD8^{+}/Foxp3^{+}$ ratio and elevated expression of PD-1 and Foxp3 as compared to T cells in the normal lung (Fig 1c). We next analyzed immune cell populations in whole lungs and detected a significant increase in the absolute number of $PD\text{-}1^{+}$ and $Foxp3^{+}$ T cells in the tumor bearing lungs, with a majority of $Foxp3^{+}$ T cells expressing PD-1 (Fig 1d,e). To assess whether other T cell inhibitory pathways were also induced in these tumors, we analyzed expression of CTLA-4, LAG-3 and Tim-3 (3). CTLA-4 was dominantly expressed by Tregs, and LAG-3 and Tim-3 were expressed by only a small percentage of PD-1 positive T cells (Fig 1e, Supplementary Fig 2a). These results suggest that the PD-1 pathway and $Foxp3^{+}$ regulatory T cell may be dominantly involved in suppressing effector T cell function in this setting. PD-1 positive T cells exhibited a memory and activation phenotype (19) (Supplementary Fig 2b), raising the possibility that EGFR-driven tumors may be characterized by host T cell exhaustion, specifically through upregulation of the PD-1 and PD-L1 interactions. Interestingly these anti-tumor immune changes were also detected in the mildy sick (based on tumor burden - lung weight) mice, suggesting these are the early events associated with oncogene expression (Supplementary Fig 3a-d).

Although PD-1 can be expressed not only by T cells, but other immune cells including B cells and macrophages after stimulation (20, 21), we were able to confirm expression of PD-1 only in T cells in this model by flow cytometry (Supplementary Fig 4).

In addition to the T cell phenotypes, we investigated how EGFR-driven tumors may induce an immunosuppressive microenvironment in the lungs. Levels of a number of immunosuppressive cytokines, growth factors and chemokines involved in immune cell accumulation were significantly higher in bronchoalveolar lavage fluid (BALF) from tumor bearing lungs compared to those from normal lungs (Fig 1f, Supplementary Fig 5a), which correlated with their mRNA expression levels in tumor bearing lungs (Fig 1a). Since soluble factors in BALFs can be produced by tumor cells as well as tumor infiltrating immune cells, we also compared the immune cell populations between normal and tumor bearing lungs by flow cytometry (gating strategy described in Supplementary methods). Among major immune cell types, the numbers of alveolar macrophages (AM) were significantly increased in tumor bearing animals, while natural killer (NK) cells were significantly decreased (Fig 1g) and showed a functionally impaired phenotype (Supplementary Fig 5b).

In vivo efficacy of PD-1 antibody blockade in mutant EGFR-driven murine lung cancer models

To confirm our findings that EGFR mutant tumors display elevated PD-L1 levels and a T cell exhaustion phenotype, and to explore whether this up-regulation drives escape from immune surveillance, we tested a rat monoclonal blocking anti-PD-1 antibody in NSCLC mouse models in which lung adenocarcinomas are driven by EGFR mutation. We generated cohorts of Del 19, TL and TD mice and induced tumor growth with doxycycline. Upon administration of clinically relevant doses of anti-PD-1 mAb (200μg (~8-10 mg/kg) 3 times a week), we detected a reduction in tumor growth in all of the EGFR mutant mouse models by MRI (Fig 2a, b), and increased apoptosis measured by Terminal deoxynucleotidyl transferase dUTP nick end labeling (TUNEL) and cleaved caspase 3 staining in TD mice (Fig 2c, 2d). Del19 mice showed the greatest tumor volume reductions (50-60 % of the baseline tumor volume after 4 weeks of therapy) (Fig 2b). TL mice showed modest tumor shrinkage response but exhibited slowed tumor growth compared to untreated mice (Fig 2b). Unlike mice with EGFR-driven tumors, transgenic mice with Kras-driven tumors did not show any significant response to the treatment with anti-PD-1 antibody (Supplementary Fig 6a-c), despite elevated PD-L1 expression (Supplementary Fig 7a,c), suggesting that factors in addition to PD-L1 influence the therapeutic activity of PD-1 antibody blockade. We also observed significantly increased survival with treatment in all three of the EGFR mutant mouse models. (Median survival treated vs untreated respectively: Del19 16.5 vs 9 weeks $p<0.0001$, TD 23.5 vs 16 $p=0.0005$, TL 23.5 vs 16.5 $p<0.0001$) (Fig 2e).

Anti-PD-1 antibody binds to activated T cells and improves effector function

Based on these findings, we explored how PD-1 blockade impacts the characteristics of host T cells and other immunosuppressive factors including cytokine production and accumulation of tumor-associated macrophages in EGFR-driven lung adenocarcinomas. Severely sick mice (based on tumor burden as determined by right lobe weights) from the two EGFR models, Del19 and TD, which showed more dramatic responses to PD-1 blockade treatment, were treated with a PD-1 blocking antibody for 1 week, and then tumor bearing lungs were harvested along with lungs from untreated severely sick mice (Fig 3a). Given that we used a rat IgG2a therapeutic antibody (clone 29F.1A12), we stained lung T cells with a secondary anti-rat IgG2a antibody as well as the same anti-PD-1 antibody used for treatment to differentiate the T cell population bound or unbound by the therapeutic antibody. The therapeutic antibody was bound to almost all of the PD-1 expressing $CD4^+$ and $CD8^+$ T cells (Fig 3b, Supplementary Fig 8a). After confirming efficient target

engagement, we next analyzed the phenotypic changes in $CD4^+$ and $CD8^+$ T cells upon PD-1 antibody blockade. Lung T cells in the treatment group showed a significantly higher $CD8^+/CD4^+$ ratio and increased numbers of total $CD8^+$ T cells as compared to those in the untreated group (Fig *3c)*. Although previous studies have shown that PD-L1 induces regulatory T cells (22), PD-1 blockade did not change the numbers of regulatory T cells (Fig 3c). T cell function was also significantly improved in terms of IFN-γ but not IL-2 production in treated lungs (Fig 3d, Supplementary Fig 8b). Consequently, IFN-γ producing $CD8^+$ T cells were significantly increased in the treatment group (Fig 3d). Histological analysis revealed increased infiltration of $CD3^+$ T cells into the tumor nodules after anti-PD-1 antibody treatment (Fig 3e), suggesting that PD-1 blockade may revive exhausted T cells, particularly cytotoxic $CD8^+$ T cells to accomplish tumor cell killing in EGFR-driven tumor models. We also explored how PD-1 blockade altered the immune microenvironment in addition to enhancing tumor apoptosis (Fig 2c,d). Among the cytokines elevated in BALFs before therapy, IL-6, TGF-β1 and progranulin (PGRN) showed a significant decrease after treatment in both of the EGFR-driven tumor models (Del19 and TD) (Fig 3f, Supplementary Fig 9a). Interestingly, the IFN-γ inducible chemokine CXCL10 was significantly elevated after treatment while its receptor, CXCR3, was expressed higher in $CD8^+$ than $CD4^+$ T cells (Supplementary Fig 9b,c). Among the immune cell populations, the total numbers of alveolar macrophages were significantly reduced in the Del19 model (Fig 3g, Supplementary Fig 10). We sorted the tumor-associated alveolar macrophages from these EGFR-driven tumor models and confirmed that they expressed *Il-6*, *Tgf-β* and *Pgrn* (data not shown).

EGFR pathway activation in human bronchial epithelial cells induces PD-L1 expression

To broaden our findings that *Pd-l1/2* expression is upregulated in response to EGFR driven oncogenic signals in mice, we compared *PD-L1* (*CD274*) and *PD-L2* (*PDCD1LG2*) expression in patient-derived established NSCLC cell lines (23), with a particular focus on lines with EGFR and KRAS mutations. EGFR and KRAS mutation are the two most prevalent drivers of lung adenocarcinomas, and tumors of these genotypes display distinct natural histories and treatment response. We observed a significant correlation among *PD-L1/2* expression with expression of *EGFR* and its ligands, markers of EGFR pathway activation (p values for individual genes are shown; combined $p<10^{-15}$) (Fig 4a). We observed a non-significant trend towards increased levels of PD-L1 in EGFR mutant lines compared to KRAS mutant lines, though the number of available cell lines with an EGFR mutation for this comparison was small (Supplementary Fig *11a*). High PD-L1 expression at the protein level was confirmed in the 6 EGFR mutant lines by flow cytometry (Fig 4, Supplementary Fig 11b). We also observed a similar result in an analysis of previously reported microarray data from patients with lung adenocarcinoma (24), in which there was a significant correlation among expression of *EGFR* and its ligands and *PD-L1* expression ($p<10^{-15}$; data not shown).

To test if ectopic expression of mutant *EGFR* is able to induce *PD-L1* expression, we stably expressed mutated *EGFR* (TD) in immortalized bronchial epithelial cells (BEAS2B). Expression of the mutated *EGFR* caused an increase in *PD-L1* levels by both real time PCR and flow cytometry in contrast to expression of $KRAS^{G12V}$, which did not induce PD-L1 (Fig 4b). This suggests that oncogenic EGFR signaling can drive *PD-L1* upregulation. Given that expression profiling of tumors suggested that the EGFR signaling pathway may positively regulate expression of PD-1 ligands, we next tested the EGFR pathway dependency of *PD-L1* expression across NSCLC cell lines. First, we evaluated the levels of PD-L1 in EGFR mutant cell lines after treatment with sub-lethal doses of the EGFR tyrosine kinase inhibitor gefitinib. Flow cytometry analysis showed a clear reduction of PD-L1 protein (Fig 4c) independent of effects on cell viability. In addition to the gefitinib sensitive

EGFR mutated lines, we also treated the gefitinib-resistant H1975 and PC-9R cell lines, which harbor an EGFR T790M mutation, with the irreversible mutant selective EGFR TKI WZ4002 (15). WZ4002, but not gefitinib decreased PD-L1 levels in H1975 cells (Fig 4d, Supplementary Fig 11c), confirming a correlation among PD-L1 levels and dependence on EGFR signaling. Although EGFR mutations predict EGFR TKI sensitivity, some EGFR wild-type cell lines also are sensitive to EGFR TKIs due to activation of the EGFR pathway by overexpression of *EGFR* or by increased production of EGFR ligands. Treatment of H358 cells, which have been previously shown to display increased EGFR signaling (25), with gefitinib resulted in PD-L1 down-regulation (Fig 4e). These findings suggest that EGFR pathway activation independent of EGFR mutation may also induce the expression of PD-L1. In addition to these studies of cell lines, we confirmed PD-L1 expression at the protein level by immunohistochemistry in mutated EGFR tumor biopsy samples obtained from patients; of the 12 EGFR mutant lung tumors we studied, 9 stained positive for PD-L1 in the tumor and/or myeloid cells (Fig 4f, Supplementary Table 1).

DISCUSSION

We have demonstrated that activation of the EGFR pathway induces *PD-L1* expression and other immunosuppressive factors to accomplish evasion of the host anti-tumor immune response. This role of EGFR signaling appears to be independent of its effects on cell proliferation and survival, suggesting an active role for the EGFR oncogene in remodeling the immune microenvironment. Pharmacological blockade of the PD-1 pathway *in vitro* using EGFR TKIs reduced *PD-L1* expression. Blocking the PD-1 pathway in EGFR mutant GEMMs resulted in tumor reduction and significantly increased overall survival. Activation of the EGFR pathway enhances susceptibility of the lung tumors to PD-1 blockade. Since PD-L1 is expressed not only by tumor cells but also macrophages and other cells of hematopoietic origin, our results suggest that combination of PD1 blockade with EGFR TKIs may be a promising therapeutic strategy to extend the duration of treatment response and delay development of resistance.

Multiple clinical studies have demonstrated clinical responses to anti-PD-1 and PD-L1 blocking antibodies in lung cancer patients (6, 7), though biomarkers associated with treatment response remain poorly understood. Preliminary results suggest that PD-L1 expression might be associated with a higher likelihood of response to PD-1 blockade, although not all PDL-1 positive tumors are sensitive (7). Similarly, we found that while EGFR and Kras mouse tumors both expressed PD-L1, only EGFR driven models responded to the PD1 blockade. Although the EGFR transgenes utilized in these murine models are derived from human cDNA sequences, genetic analysis of human NSCLCs typically reveals the presence of large numbers of somatically mutated proteins that might be targets for anti-tumor T cells (26). Future studies will investigate the antigens triggering T cell responses in the murine EGFR-driven lung cancer models.

A growing body of evidence suggests that several oncogenes may directly influence the tumor microenvironment through regulating the expression of soluble ligands and cytokines (27). Secretion of these factors may act in paracrine to stimulate and transform neighboring cells, while recruiting myeloid derived suppressor cells (MDSC) and Tregs, which are associated with a poor prognosis, in contrast to the tumor infiltrating cytotoxic lymphocytes, which are associated with a better prognosis (28). EGFR mutant mice exhibited an impaired immune response that involved not only PD-1 activation, but also the upregulation of IL-6, TGF-β1 and progranulin (PGRN). Previous reports have shown that these cytokines promote tumor growth and cause immune suppression (29-31) and, in the case of TGF-β, also support tumor metastasis by inducing epithelial to mesenchymal transition, which has been associated with resistance to cytotoxic T cell killing (32, 33). Our results together with

previous reports suggest that EGFR-driven tumors create a favorable microenvironment for proliferation of tumor cells not only by inducing PD-L1 expression, but also through the production of cytokines and immunosuppressive cells such as regulatory T cells and macrophages. PD-1 blockade reduces tumor burden both by eliminating tumor cells as well as reducing both the levels of tumor promoting cytokines and the numbers of immunosuppressive cells. These findings also suggest that a part of the mechanism of action of tyrosine kinase inhibitors in NSCLCs may involve reversing the EGFR pathway driven immunosuppression in the tumor microenvironment in addition to the well-understood effects on EGFR-driven intracellular signaling.

In murine melanoma models and possibly melanoma patients, the combination of anti-PD-1 and CTLA-4 antibodies may be more effective than either agent alone due to the complementary functional roles of these two negative immune checkpoints (34, 35). PD-1 blockade in the EGFR-driven mouse lung cancer models did not alter the numbers of Tregs that express high levels of CTLA-4, suggesting a rationale for combined antibody treatment. Additional work is required to explore this possibility and other potential combinatorial therapies, and to delineate the differences in treatment response among the varying EGFR mutations and other oncogene activated models.

MATERIALS AND METHODS

Microarray data analysis

For gene expression analysis of NSCLC cell lines, RMA normalized expression data were downloaded from the cancer cell line encyclopedia (CCLE) (www.broadinstitute.org/ccle). Expression data from wild type and EGFR transgenic mice were obtained from a previous study (18) and converted into log2 values. Pearson correlation coefficient p values were calculated by comparing expression values for each transcript over all samples to either PD-L1 or PD-1 expression.

Cell line experiments

Beas2B cells (ATTC # CRL9609) were grown in Bronchiolar epithelial cell basal medium (Lonza # CC-3170), and maintained with Hepes buffer solution, trypsin, and trypsin neutralizing solution (Lonza #CC-5034). Mutations in EGFR or Kras were introduced and cloned into the PLCPX vector (Addgene). Clones stably expressing the mutant EGFR or Kras were selected with puromycin (2 μg/ml) for 3 days. Other cell lines were purchased from ATCC. Genotypes of the patient derived NSCLC cells are as follows: PC9-del 19, and HCC827-del 19, H1975- L858R, T790M, PC9R-del 19, T790M. All cell lines were cultured in RPMI1640 (Corning) supplemented with 10% heat inactivated FBS, 100 units/ml penicillin, 100 mg/ml streptomycin and 10 mM HEPES. For PD-L1 expression analysis, untreated cells and gefitinib or WZ4002 treated cells were stained with anti PD-L1 antibody (29E.2A3) and isotype control (Biolegend) and then stained with Annexin V and 7-AAD (eBioscience); PD-L1 levels were determined for the Annexin V and 7-AAD double negative population using a BD Canto II cytometer equipped with Diva software (BD Biosciences). The final analysis and graphical output were performed using Flowjo (Treestar). Treatment doses that did not compromise cell survival were determined with a CellTiter-Glo Luminescent Cell Viability Assay (Promega) after 72 hours.

Realtime PCR

Total RNA was extracted using Trizol (Invitrogen, Grand Island, NY #15596018) followed by RNA cleanup (QIAGEN, Valencia, CA #74204). cDNA were prepared from total RNA preps using the High-capacity RNA-cDNA kit (Invitrogen # 4377474). Real time assays were done using Taqman real time probes (Invitrogen) for human PDL1/CD274

(Hs01125301_m1) and GUSB (Hs00939627_m1) using 40ng cdna. Triplicates were run for each sample. GUSB was used as internal control and ΔΔCT method was used for relative mRNA calculations.

Mouse husbandry and breeding

All EGFR transgenic mice carrying tetracycline inducible human EGFR cDNA were previously generated, crossed with CC10-RTTA mice expressing reverse tetracycline activator from lung Clara cell CC10 promoter as previously described (13-15), and maintained in mixed (C57Bl/6, FVB, and S129) background. Double positive progeny were fed with doxycycline diet starting at 5-6 weeks of age for the induction of tumors and maintained on doxycyline throughout the study. All breedings and *in vivo* experiments were performed with the approval of the DFCI Animal Care and Use Committee.

Antibody dosing

Mice received rat anti-PD-1 monoclonal antibody (clone 29F.1A12) by intra-peritoneal injections (200 μg in PBS per dose (8-10 mg/kg), 3 times a week), as described (36). Control mice received similar injections of 200μg of rat IgG2a isotype control in PBS (BioXcell).

MRI tumor volume quantification and survival

Tumor volume quantifications were performed using the 3D-Slicer software described in detail in supplementary methods. Survival curves were generated by pooling animals that were sacrificed due to heavy tumor burden or were otherwise found dead.

Bronchoalveolar lavage fluid (BAL) fluid collection and Cytokine measurement

1ml PBS was injected into the trachea to inflate the lungs, which were then aspirated and frozen. Cytokine concentrations in serum and BALFs were measured with ELISA kits for mouse IL-6, TGF-beta1, PGRN, VEGF, GM-CSF, MFG-E8, CCL17 (R & D systems) and CCL2, CCL5, and CXCL10 (eBioscience).

Histology and immunohistochemistry

Mice were classified at euthanasia into mild or severe pulmonary pathology based on lung weights: Severe(s), total right lung weight ≧ 650 mg; mild (m), total right lung weight < 650 mg. Lungs were inflated with 10% formalin and embedded in paraffin. 5 μm sections were cut for hematoxylin/eosin staining and immunohistochemistry. Anti-cleaved caspase 3 mAb (Abcam #2302) was used at 1/20 dilution, anti-CD3 mAb at 1/50 dilution (Dako # A0452). TUNEL assay was performed per the manufacturer's instructions (Millipore # 17-141). The numbers of positive cells from the tumor nodules of similar size taken at the 20X objective were counted. Comparisons of treatment groups were performed using T tests. PD-L1 immunohistochemistry was performed using the automated immunostainer (Ventana, Tucson, AZ) on patient slides and manually on the mouse slides at 10μg/ml concentration using anti-PD-L1 antibody as described (37). PD-L1 knockout mouse tissues were used as negative control for PD-L1 IHC (Supplementary fig 7b).

Total lung cell and tumor infiltrating cell characterization

Briefly, mice were sacrificed, and blood was collected through cardiac puncture; lungs were then perfused with cold PBS containing 5 mM EDTA from the right ventricle after collecting BAL fluid. Whole normal or tumor bearing lung was resected and one left lobe and five right lobes were used for histological and flow cytometry analysis, respectively. Whole right lobes were shredded into small pieces and incubated in collagenase containing buffer: 100 units/ml of collagenase type IV (Invitrogen), 10 μg/ml of DNase I (Roche), and

10% FBS in RPMI1640 medium for 45 min. After incubation, cells were treated with RBC lysis buffer and passed through cell strainer to remove debris. The cell pellet was dissolved by 2% FCS in HBSS and used for flow cytometry analysis. For counting absolute number of immune cell populations, AccuCheck Counting Beads (Molecular probes) were used according to the manufacturer's protocol. For intracytoplasmic cytokine staining, lung cells were fractionated over cell separation media-Optiprep (Sigma) and buffered saline with Tricine (Sigma) per the manufacturer's instructions (Axis-Shield, Application Sheet C43). Isolated mononuclear cells were stimulated with 50 ng/ml PMA (Sigma) and 500 ng/ml Ionomycin (Sigma) for 4 h in the presence of Golgi plug (BD Biosciences). Isolated cells were stained with LIVE/DEAD fixable dead cell stain kit (invitrogen). Cells were subsequently stained with anti-Rat IgG2a (clone R2a-21B2) (eBioscience) to check anti-PD-1 blocking antibody binding and then with mAbs directed against several surface antigens listed in supplemental methods. Fixation/permeabilization buffers (eBioscience) were used for intracellular staining. Acquisition of eight color samples was performed on a BD Canto II cytometer equipped with Diva software and analyzed using Flowjo. Gating strategy in this study is shown in supplemental methods.

Statistical Analysis

All numerical data are presented as mean±SD. Data were analyzed using unpaired two-tailed Student's t test. P values for the survival curves have been calculated using a log rank test.

Supplementary Material

Refer to Web version on PubMed Central for supplementary material.

Acknowledgments

We thank Christine Lam for help with processing the tissues, Heather Sun and Mei Zhang for help with the tissue stainings, PD-L1 knock-out mouse tissues were kindly provided by Dr Arlene Sharpe at Harvard Medical School. This work is supported by the NIH (CA122794, CA140594, CA163896, CA166480, CA154303, and Lung SPORE P50CA090578), United against Lung Cancer, American Lung Association, and Susan Spooner Research Fund to KKW, NCI R01CA143083, the Leukemia & Lymphoma Society, and the Research Foundation for the Treatment of Ovarian Cancer to GD, Margaret A. Cunningham Immune Mechanisms in Cancer Research Fellowship Award to SK, and NCI 1K08CA163677 to PSH.

REFERENCES

1. Hanahan D, Weinberg RA. Hallmarks of cancer: the next generation. Cell. 2011; 144:646–74. [PubMed: 21376230]
2. Dunn GP, Bruce AT, Ikeda H, Old LJ, Schreiber RD. Cancer immunoediting: from immunosurveillance to tumor escape. Nat Immunol. 2002; 3:991–8. [PubMed: 12407406]
3. Pardoll DM. The blockade of immune checkpoints in cancer immunotherapy. Nat Rev Cancer. 2012; 12:252–64. [PubMed: 22437870]
4. Hodi FS, O'Day SJ, McDermott DF, Weber RW, Sosman JA, Haanen JB, et al. Improved survival with ipilimumab in patients with metastatic melanoma. N Engl J Med. 2010; 363:711–23. [PubMed: 20525992]
5. Sharpe AH, Wherry EJ, Ahmed R, Freeman GJ. The function of programmed cell death 1 and its ligands in regulating autoimmunity and infection. Nat Immunol. 2007; 8:239–45. [PubMed: 17304234]
6. Brahmer JR, Tykodi SS, Chow LQ, Hwu WJ, Topalian SL, Hwu P, et al. Safety and activity of anti-PD-L1 antibody in patients with advanced cancer. N Engl J Med. 2012; 366:2455–65. [PubMed: 22658128]

7. Topalian SL, Hodi FS, Brahmer JR, Gettinger SN, Smith DC, McDermott DF, et al. Safety, activity, and immune correlates of anti-PD-1 antibody in cancer. N Engl J Med. 2012; 366:2443–54. [PubMed: 22658127]
8. Parsa AT, Waldron JS, Panner A, Crane CA, Parney IF, Barry JJ, et al. Loss of tumor suppressor PTEN function increases B7-H1 expression and immunoresistance in glioma. Nat Med. 2007; 13:84–8. [PubMed: 17159987]
9. Zaiss DM, van Loosdregt J, Gorlani A, Bekker CP, Grone A, Sibilia M, et al. Amphiregulin enhances regulatory T cell-suppressive function via the epidermal growth factor receptor. Immunity. 2013; 38:275–84. [PubMed: 23333074]
10. Pivarcsi A, Muller A, Hippe A, Rieker J, van Lierop A, Steinhoff M, et al. Tumor immune escape by the loss of homeostatic chemokine expression. Proc Natl Acad Sci U S A. 2007; 104:19055–60. [PubMed: 18025475]
11. Ohashi K, Maruvka YE, Michor F, Pao W. Epidermal growth factor receptor tyrosine kinase inhibitor-resistant disease. J Clin Oncol. 2013; 31:1070–80. [PubMed: 23401451]
12. Imielinski M, Berger AH, Hammerman PS, Hernandez B, Pugh TJ, Hodis E, et al. Mapping the hallmarks of lung adenocarcinoma with massively parallel sequencing. Cell. 2012; 150:1107–20. [PubMed: 22980975]
13. Ji H, Li D, Chen L, Shimamura T, Kobayashi S, McNamara K, et al. The impact of human EGFR kinase domain mutations on lung tumorigenesis and in vivo sensitivity to EGFR-targeted therapies. Cancer Cell. 2006; 9:485–95. [PubMed: 16730237]
14. Li D, Shimamura T, Ji H, Chen L, Haringsma HJ, McNamara K, et al. Bronchial and peripheral murine lung carcinomas induced by T790M-L858R mutant EGFR respond to HKI-272 and rapamycin combination therapy. Cancer Cell. 2007; 12:81–93. [PubMed: 17613438]
15. Zhou W, Ercan D, Chen L, Yun CH, Li D, Capelletti M, et al. Novel mutant-selective EGFR kinase inhibitors against EGFR T790M. Nature. 2009; 462:1070–4. [PubMed: 20033049]
16. Ercan D, Xu C, Yanagita M, Monast CS, Pratilas CA, Montero J, et al. Reactivation of ERK Signaling Causes Resistance to EGFR Kinase Inhibitors. Cancer Discov. 2012
17. Chen Z, Sasaki T, Tan X, Carretero J, Shimamura T, Li D, et al. Inhibition of ALK, PI3K/MEK, and HSP90 in murine lung adenocarcinoma induced by EML4-ALK fusion oncogene. Cancer Res. 2010; 70:9827–36. [PubMed: 20952506]
18. Weaver Z, Difilippantonio S, Carretero J, Martin PL, El Meskini R, Iacovelli AJ, et al. Temporal molecular and biological assessment of an erlotinib-resistant lung adenocarcinoma model reveals markers of tumor progression and treatment response. Cancer Res. 2012; 72:5921–33. [PubMed: 22969147]
19. Wherry EJ, Teichgraber V, Becker TC, Masopust D, Kaech SM, Antia R, et al. Lineage relationship and protective immunity of memory CD8 T cell subsets. Nat Immunol. 2003; 4:225–34. [PubMed: 12563257]
20. Francisco LM, Sage PT, Sharpe AH. The PD-1 pathway in tolerance and autoimmunity. Immunol Rev. 2010; 236:219–42. [PubMed: 20636820]
21. Huang X, Venet F, Wang YL, Lepape A, Yuan Z, Chen Y, et al. PD-1 expression by macrophages plays a pathologic role in altering microbial clearance and the innate inflammatory response to sepsis. Proc Natl Acad Sci U S A. 2009; 106:6303–8. [PubMed: 19332785]
22. Francisco LM, Salinas VH, Brown KE, Vanguri VK, Freeman GJ, Kuchroo VK, et al. PD-L1 regulates the development, maintenance, and function of induced regulatory T cells. J Exp Med. 2009; 206:3015–29. [PubMed: 20008522]
23. Barretina J, Caponigro G, Stransky N, Venkatesan K, Margolin AA, Kim S, et al. The Cancer Cell Line Encyclopedia enables predictive modelling of anticancer drug sensitivity. Nature. 2012; 483:603–7. [PubMed: 22460905]
24. Shedden K, Taylor JM, Enkemann SA, Tsao MS, Yeatman TJ, Gerald WL, et al. Gene expression-based survival prediction in lung adenocarcinoma: a multi-site, blinded validation study. Nat Med. 2008; 14:822–7. [PubMed: 18641660]
25. Yonesaka K, Zejnullahu K, Lindeman N, Homes AJ, Jackman DM, Zhao F, et al. Autocrine production of amphiregulin predicts sensitivity to both gefitinib and cetuximab in EGFR wild-type cancers. Clin Cancer Res. 2008; 14:6963–73. [PubMed: 18980991]

26. Matsushita H, Vesely MD, Koboldt DC, Rickert CG, Uppaluri R, Magrini VJ, et al. Cancer exome analysis reveals a T-cell-dependent mechanism of cancer immunoediting. Nature. 2012; 482:400–4. [PubMed: 22318521]
27. Shang B, Zhang G, Pan Y, Zhou Q. Deciphering the Key Features of Malignant Tumor Microenvironment for Anti-cancer Therapy. Cancer Microenviron. 2012; 5:211–23. [PubMed: 22592483]
28. Whiteside TL. The tumor microenvironment and its role in promoting tumor growth. Oncogene. 2008; 27:5904–12. [PubMed: 18836471]
29. Gao SP, Mark KG, Leslie K, Pao W, Motoi N, Gerald WL, et al. Mutations in the EGFR kinase domain mediate STAT3 activation via IL-6 production in human lung adenocarcinomas. J Clin Invest. 2007; 117:3846–56. [PubMed: 18060032]
30. Frampton G, Invernizzi P, Bernuzzi F, Pae HY, Quinn M, Horvat D, et al. Interleukin-6-driven progranulin expression increases cholangiocarcinoma growth by an Akt-dependent mechanism. Gut. 2012; 61:268–77. [PubMed: 22068162]
31. Flavell RA, Sanjabi S, Wrzesinski SH, Licona-Limon P. The polarization of immune cells in the tumour environment by TGFbeta. Nat Rev Immunol. 2010; 10:554–67. [PubMed: 20616810]
32. Kudo-Saito C, Shirako H, Takeuchi T, Kawakami Y. Cancer metastasis is accelerated through immunosuppression during Snail-induced EMT of cancer cells. Cancer Cell. 2009; 15:195–206. [PubMed: 19249678]
33. Akalay I, Janji B, Hasmim M, Noman MZ, Andre F, De Cremoux P, et al. Epithelial-to-mesenchymal transition and autophagy induction in breast carcinoma promote escape from T-cell-mediated lysis. Cancer Res. 2013; 73:2418–27. [PubMed: 23436798]
34. Curran MA, Montalvo W, Yagita H, Allison JP. PD-1 and CTLA-4 combination blockade expands infiltrating T cells and reduces regulatory T and myeloid cells within B16 melanoma tumors. Proc Natl Acad Sci U S A. 2010; 107:4275–80. [PubMed: 20160101]
35. Wolchok JD, Kluger H, Callahan MK, Postow MA, Rizvi NA, Lesokhin AM, et al. Nivolumab plus Ipilimumab in Advanced Melanoma. N Engl J Med. 2013
36. Barber DL, Wherry EJ, Masopust D, Zhu B, Allison JP, Sharpe AH, et al. Restoring function in exhausted CD8 T cells during chronic viral infection. Nature. 2006; 439:682–7. [PubMed: 16382236]
37. Chen BJ, Chapuy B, Ouyang J, Sun HH, Roemer MG, Xu ML, et al. PD-L1 Expression Is Characteristic of a Subset of Aggressive B-cell Lymphomas and Virus-Associated Malignancies. Clin Cancer Res. 2013

SIGNIFICANCE

We show that autochthonous EGFR-driven lung tumors inhibit anti-tumor immunity by activating the PD-1/PD-L1 pathway to suppress T cell function and increase levels of pro-inflammatory cytokines. These findings indicate that EGFR functions as an oncogene through non-cell autonomous mechanisms and raise the possibility that other oncogenes may drive immune escape.

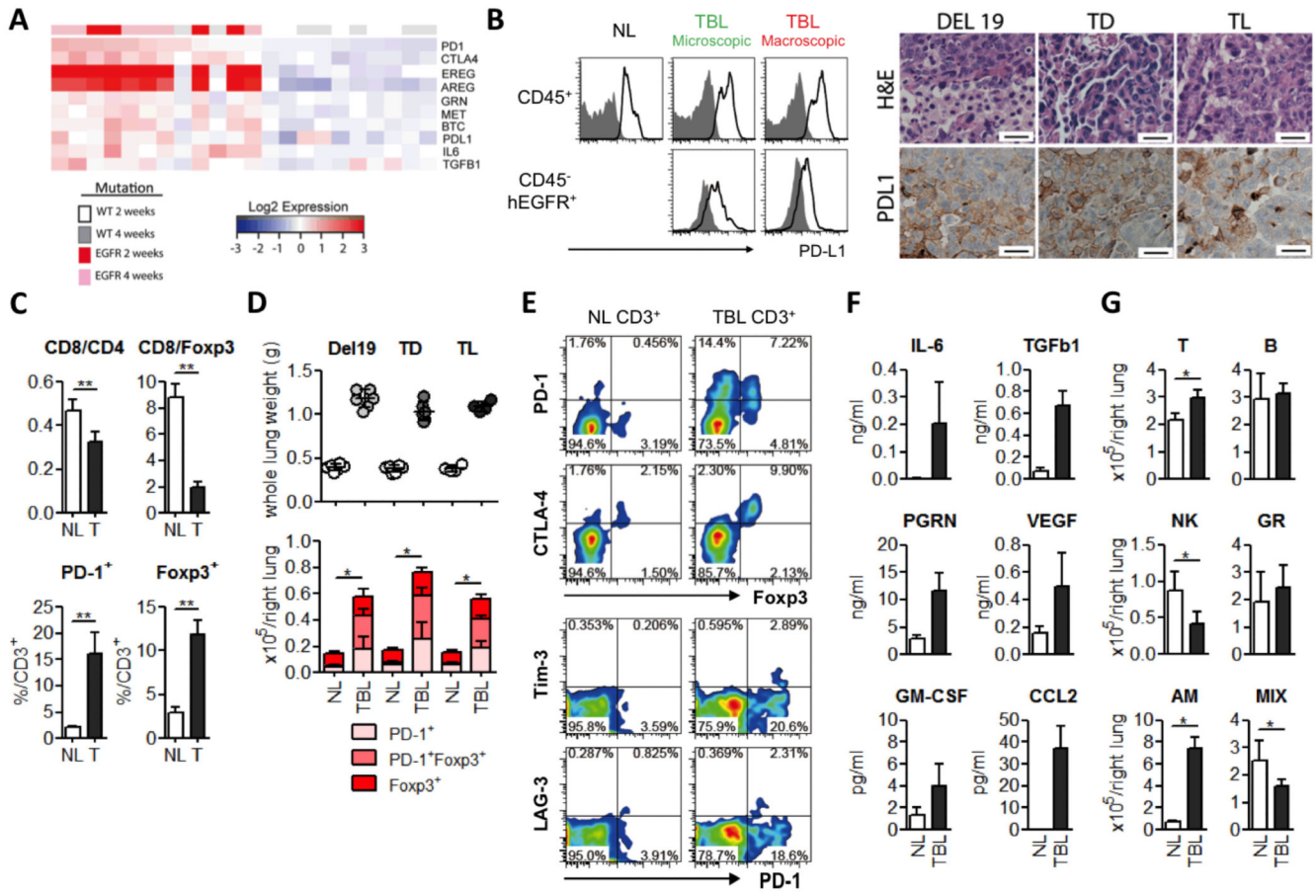

Figure 1. Activation of the EGFR pathway in bronchial epithelial cells leads to an immunosuppressive lung microenvironment

(a) Microarray expression profiling analysis of lung tumors from mice with EGFR T790M, L858R (TL) or control lungs focusing on *Pd-1*, *Ctla-4*, *Pd-l1*, the EGFR ligands eregulin (*Ereg*), amphiregulin (*Areg*), and betacellulin (*Btc*), and the cytokines *Tgf-ß1*, granulin (*Grn*), and interleukin-6 (*Il6*). 2 and 4 week time points indicate the time between the induction of the transgene with doxycycline and subsequent euthanasia. EGFR mutant vs WT for the gene set shown $p=3\times10^{-20}$ (b) Left: Surface PD-L1 expression on $CD45^+$ hematopoietic cell population and $CD45^-$ human $EGFR^+$ cells (tumor cells) was evaluated by FACS. PD-L1 and isotype control staining are shown with the clear black and gray filled lines respectively for normal lung (NL) and tumor bearing lung (TBL) with either microscopic disease or macroscopic nodules. Right: Representative images from the lungs of Del19, TD and TL mice stained for hematoxylin and eosin (H&E) and PD-L1. Scale bars show 100μm for all panels. (c) $CD8^+/CD4^+$ and $CD8^+/Foxp3^+$ ratios and PD-1 and Foxp3 positive frequencies in total $CD3^+$ T cells from NL and tumor (T) from T790M L858R (TL) mice: n=4) *p<0.01. (d) Lung weights of control mice and mice carrying tumors driven by Del19, TD or TL. Quantitative analysis of PD-1 and Foxp3 positive T cells (con and TL: n=4, con and Del, con and TD: n=6) * p<0.05 (NL vs TBL for each group; $PD\text{-}1^+$, $PD\text{-}1^+Foxp3^+$ and $Foxp3^+$) (e) Co-expression of immune suppressive receptors; Foxp3, PD-1, LAG-3, and Tim-3 in $CD3^+$ T cells. (f). Concentration of cytokines IL-6, TGF-b1, progranulin (PRGN), vascular endothelial growth factor (VEGF), granulocyte-macrophage colony stimulating factor (GM-CSF), and CCL2 in BALFs from NL (white bars) and TBL from TL mice (black bars) (con and TL: n=6). NL vs TBL for all cytokines, p<0.02 (g)

Immune cell populations; T cell, B cell, NK cell, granulocytes (GR), alveolar macrophages (AM) and mixed populations ($CD11b^{+}F4/80^{+}$ population) (the method to identify each population was shown in supplementary methods) in NL and TBL (con and TL: n=4) * $p<0.05$

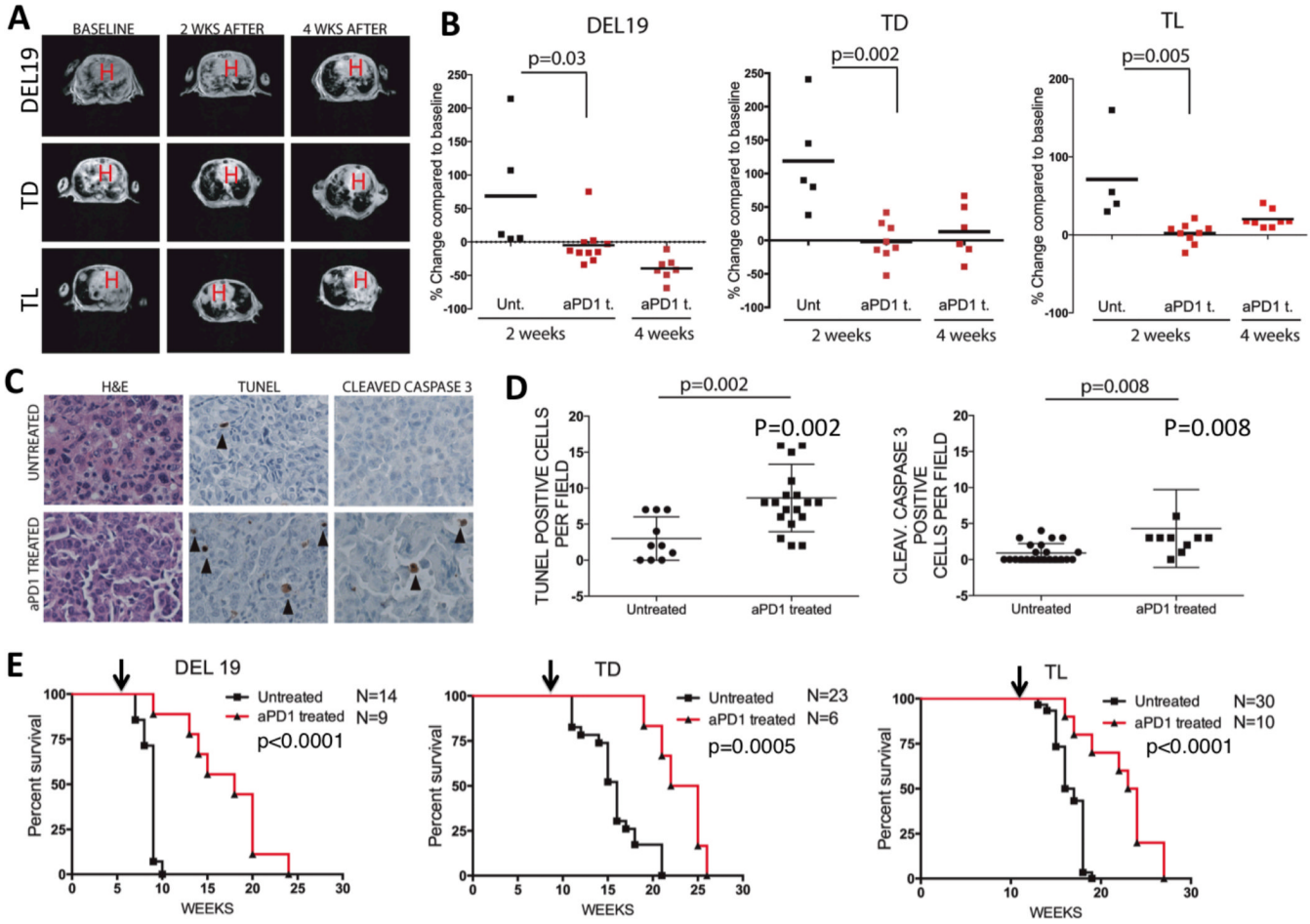

Figure 2. In vivo efficacy of PD-1 antibody blockade in EGFR mutant murine lung cancer models

The anti-tumor effects of anti-PD-1 antibodies in mouse models of EGFR driven lung cancers (a-e). (a) Tumor volume changes by MRI at varying time points; baseline, 2, and 4 weeks after treatment of the indicated genotypes of mice. H indicates location of the heart. (b) Quantification of tumor volume changes as compared to baseline tumor volumes in the mice that were treated with anti-PD1 antibody (aPD1 t.) or left untreated (Unt,). (c) Representative images of lung sections from tumor bearing mice (TD) that were either treated with anti-PD-1 antibody (aPD1 t.) for 1 week or left untreated. Sections were stained for H&E, TUNEL, and cleaved caspase 3. Scale bars represent 25 μm for all panels. (d) Quantification of TUNEL and caspase 3 stainings respectively. Data points indicate total positive signal per tumor field. For TUNEL: n=3 for untreated and n=4 for PD-1 treated mice; for cleaved caspase 3: n=6 for untreated and n=3 for PD-1 treated mice). (e) Kaplan Meier survival analysis of the anti-PD-1 antibody treated or untreated mice bearing EGFR driven tumors. Treatments were started after tumors were confirmed with MRI at the time points indicated by arrows for each of the mouse lines.

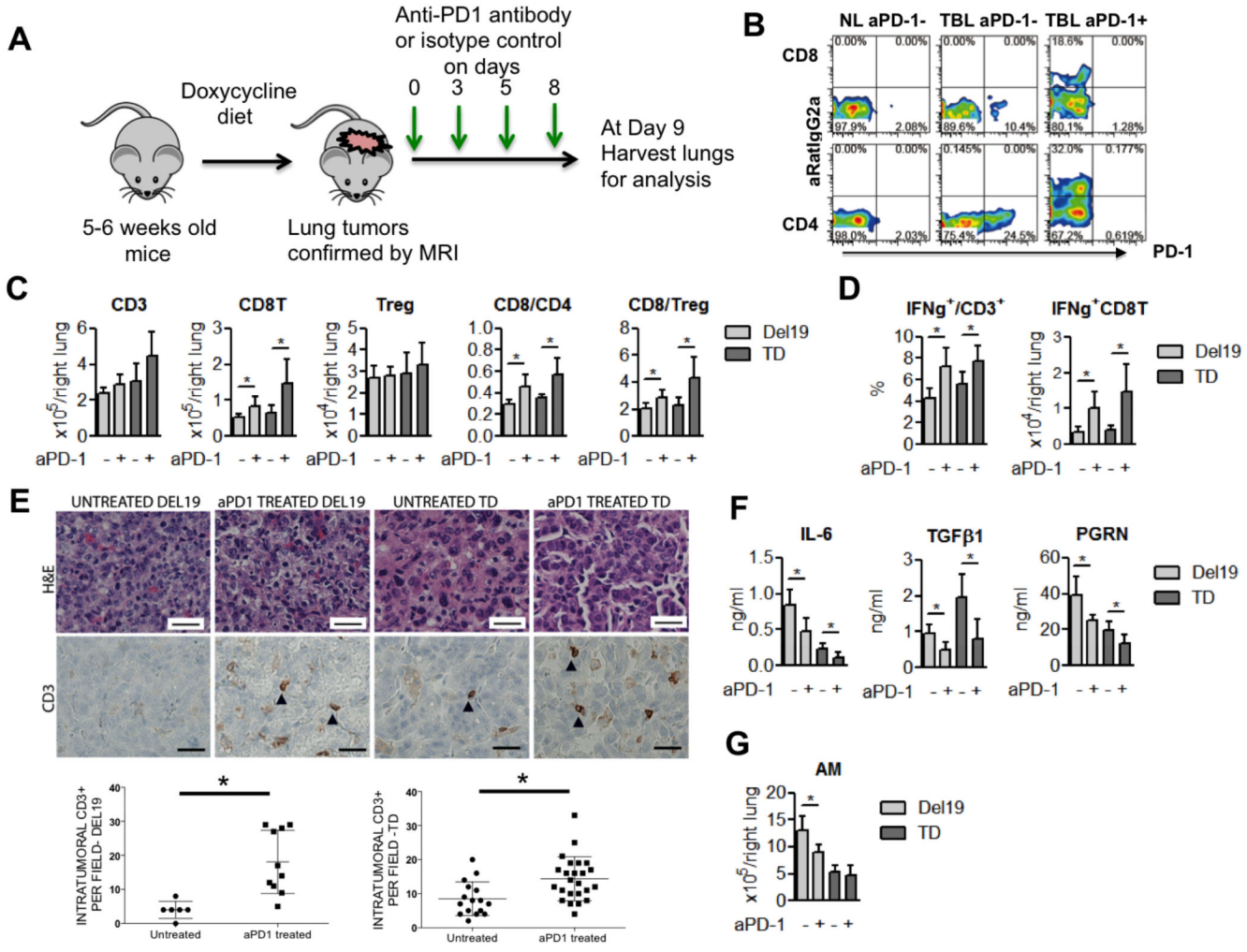

Figure 3. Anti-PD-1 antibody binds to activated T cells and improves effector function

(a) Schematic of the short term in vivo treatment of mice with anti-PD-1 antibodies after tumor burden was confirmed by MRI imaging. Each group was treated either with isotype control (untreated) or anti-PD-1 antibody on Days 0, 3, 5 and 8 (4 doses), and then at day 9 mice were sacrificed for analysis. (b) Representative flow cytometry results of PD-1$^+$ or RatIgG2a$^+$ (therapeutic anti-PD-1 antibody binding) in CD4$^+$ and CD8$^+$ T cells, anti-PD1 antibody treated mouse (+ aPD1), control antibody treated mouse (- aPD1) (c) Changes in total T cell (CD3), CD8$^+$ T cells, and Tregs, and ratios of CD8/CD4 and CD8/Treg after PD-1 blockade. (d) Enhancement of effector T cell function (IFN-γ production) by PD-1 antibody blockade. (e) CD3 immunohistochemistry (top) and quantification of intra-tumoral CD3+ cells per high power field in untreated and PD-1 antibody treated tumors (bottom). Scale bars indicate 25 μm for all panels. Each point on the graph represents counts from single tumor nodule. For del19, N= 2 for untreated, n=5 for anti-PD-1 antibody treated mice. For TD, n=4 for untreated and n=5 for anti-PD-1 antibody treated mice. P=0.01 for both CD3 graphs. (e) Enhancement of T cell function represented as IFN-γ production by PD-1 antibody blockade. (f) Concentration of the cytokines IL-6, TGF-β1, and PRGN in BALFs. (g) Absolute number of alveolar macrophages in lungs from Del. For all bar graphs in this figure Del 19 (untreated and treated: n=6 and n=7) and TD (untreated and treated: n=6 and n=6) * $p<0.05$

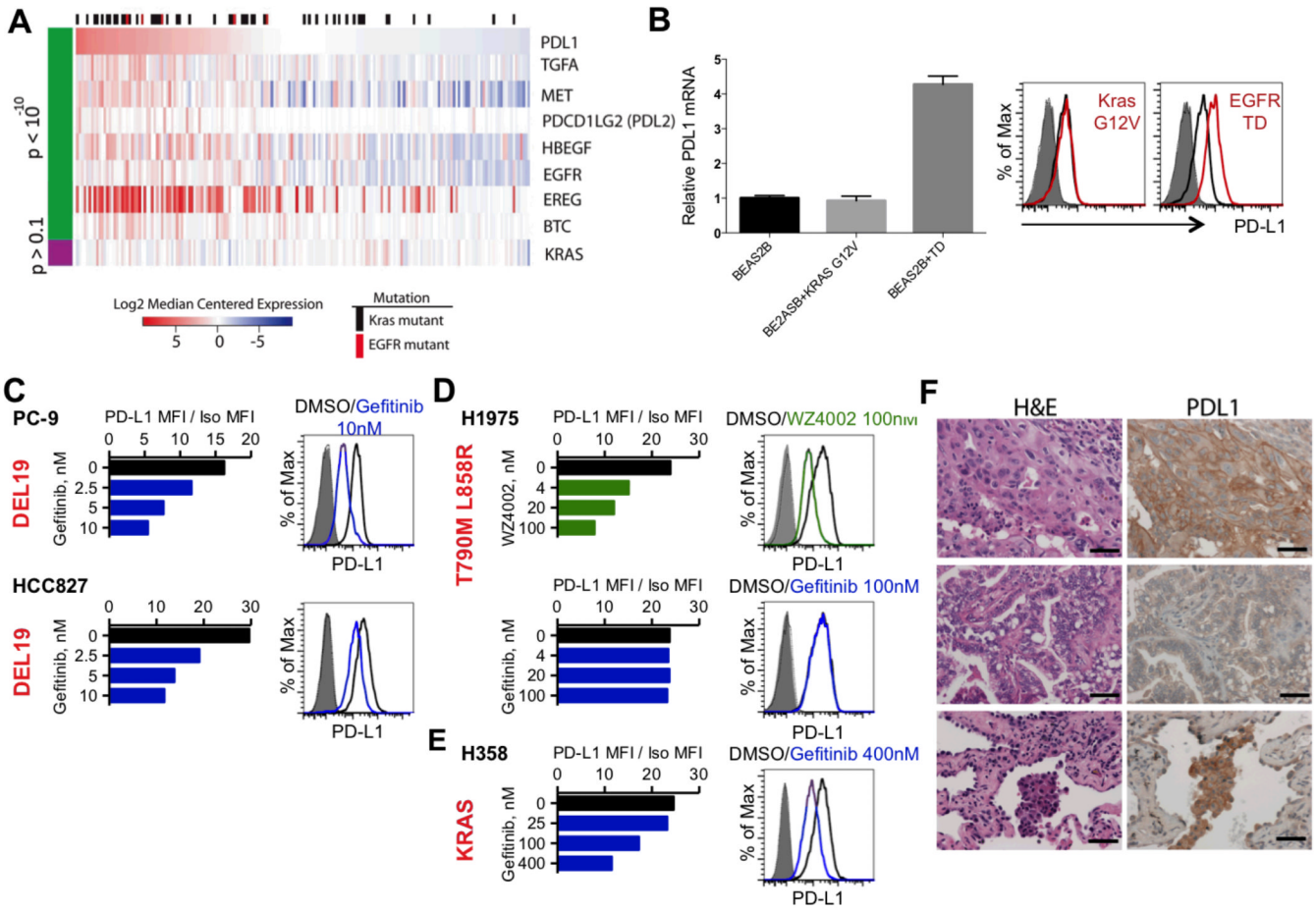

Figure 4. EGFR pathway activation in human bronchial epithelial cells induces PD-L1 expression

(a) Microarray expression profiling analysis of established cell lines from human NSCLC patients. Black and red bars indicate identified Kras or EGFR mutations respectively. TGF-alpha, met proto-oncogene (MET), heparin-binding EGF-like growth factor (HBEGF), EREG and BTC are EGFR ligands. (b) PD-L1 up-regulation in BEAS-2B bronchial epithelial cell lines transduced with vectors encoding Kras mutation (G12V) or EGFR mutation (T790M-Del19), as assessed by qPCR and flow cytometry (c-e). Reduction of PD-L1 expression in NSCLC cell lines 72 hours after EGFR TKI treatment at the indicated concentrations (in the absence of drug-induced apoptosis) (c) EGFR-del19 mutant PC-9 and HCC827 NSCLCs (d), Gefitinib resistant H1975 NSCLC (e) EGFR wild type Kras mutant H358 NSCLC. Representative results from 3 independent experiments are shown. (f) Sections of formalin fixed patient tumors carrying EGFR mutations stained with H&E or PD-L1. Top panel, high expression on tumor cell membrane; middle panel, low expression on membrane; bottom panel, expression on macrophages. Scale bars show 100 μm.